Fe-Nanoparticle Effect on Polypropylene for Effective Radiation Protection. Simulation and theoretical study.

Marwan Alshipli
Aqaba University of Technology
MUTAZ Aladailah (aladailehmotaz@gmail.com)
Ural Federal University named after the first President of Russia B N Yeltsin: Ural'skij federal'nyj universitet imeni pervogo Prezidenta Rossii B N El'cina https://orcid.org/0000-0002-8675-0608
M.W. Marashdeh
Imam Muhammad Ibn Saud Islamic University
H. Akhdar
Imam Muhammad Ibn Saud Islamic University
O.L. Tashlykov
Ural Federal University named after the first President of Russia B N Yeltsin: Ural'skij federal'nyj universitet imeni pervogo Prezidenta Rossii B N El'cina
Walaa Al-Tamimi
The University of Jordan

Research Article

Keywords: Geant4 code, EpiXS programme, Fe-Nanoparticle, Polypropylene, Radiation shielding

Posted Date: October 17th, 2022

DOI: https://doi.org/10.21203/rs.3.rs-2132034/v1

Fe-Nanoparticle Effect on Polypropylene for Effective Radiation Protection. Simulation and theoretical study.

Marwan Alshipli [1], M. W. Aladailah [2], M.W.Marashdeh [3], H. Akhdar [3], O.L. Tashlykov [2], Al-Tamimi Walaa [4]

[1] Medical Imaging and Radiography Department, Aqaba University of Technology, Aqaba, Jordan.

[2] Ural Federal University, 19 Mira St., Yekaterinburg, Russia

[3] Department of Physics, College of Science, Imam Mohammad Ibn Saud Islamic University (IMSIU), Riyadh, 11623, Saudi Arabia

[4] The University of Jordan, Amman 11942, Jordan.

Highlights

- Novel polymer nanocomposites materials have been examined.
- Gamma-neutron shielding capabilities were studied for polymer nanocomposite materials based on polypropylene.
- EpiXS data were compared with the simulation findings.
- The PP-Fe_5 sample has excellent gamma ray shielding properties.

Abstract

In this study, polymer nanocomposite materials based on polypropylene and iron nanoparticles are evaluated for their gamma-neutron shielding capabilities. The chemical composition of these materials is (100-x) PP-Fe_x, (where x = 0.1, 0.3, 0.5, 1, 2 and 5 weight percent). Using the Geant4 Monte Carlo code, the mass attenuation coefficient(MAC), a crucial parameter for studying the gamma-ray shielding capabilities, was determined for the proposed polymer samples in the photon energy range of 30-2000 KeV. The results were compared to those predicted by the EpiXS programme. The values of the Geant4 code and the EpiXS software were

both found to be in excellent agreement. The linear attenuation coefficients, electron density, effective atomic number, and half value layer for all the concerned samples were then determined for each sample using the mass attenuation coefficient values. Additionally, the polymer samples' neutron shielding properties were evaluated by estimating both the fast neutron removal cross-section and the mean free path of the fast neutron in the energy ranging between 0.25-5.5 KeV. The findings show that as the polymer sample's Fe nanoparticle content rises, the PP-Fe polymer samples' gamma-ray shielding efficacy changes. Among the examined glasses, the PP-Fe_5 polymer sample offers the best gamma-ray shielding ability. Finally, the PP-Fe_5 polymer sample containing 5 mol% of Fe, has the highest $\sum R$ value (1.10650 cm^{-1}) and the lowest value of the fast neutron mean free path. This means that the $PPFe_5$ possesses better neutron shielding efficiency.

Keywords: Geant4 code; EpiXS programme; Fe-Nanoparticle; Polypropylene; Radiation shielding

1. Introduction

Numerous techniques, including optimizing the efficient compositions of radiation-protective materials, can be used to apply the optimization principle to personnel radiological protection [1, 2]. Shielding the environment and humans is therefore very important. Researchers have investigated several shielding materials to attenuate the ionizing radiation [3-5]. The high attention ability of lead and concrete against ionizing radiation makes them traditional shielding materials. However, researchers face several challenges when developing shielding materials, including materials toxicity, attenuation abilities, weight, mechanical stability, and cost [6, 7].

The use of lead and concrete as radiation shielding materials protects humans from being affected by the harmful effects of radiation. But, the heterogeneous nature of lead and its

toxicity, as well as moisture variation and cracking in concrete make it challenging to use as radiation protection material [7-9]. Furthermore, traditional radiation shielding materials produce more penetrative secondary radiation, thus requiring additional shielding, increasing cost and weight. As a result, researchers have focused on developing shielding materials that are efficient, cost-effective, lightweight, and flexible [10-12].

The development of free lead shielding materials was therefore pursued to eliminate environmental disposal concerns associated with lead-based materials. The development of materials that can effectively attenuate ionizing radiation has been made possible by the development of polymer composites. [13-16]. Because polymers are lightweight, durable, flexible, and have superior physical, mechanical, and high attenuation properties, they are promising alternatives to traditional radiation shielding materials [16, 17]. In addition, polymers can readily be doped with high effective atomic number materials to produce composites that are more effective radiation shields [18].

Recently, polymer nanocomposite materials have been used in medicine for a wide range of diagnostic and therapy areas [19]. In radiation protection fields, polymer nanocomposites reinforced for their lightweight, mechanical stability, and good radiation attenuation ability have attracted great interest [20-22]. Since nanoparticles have a larger cross-section than micro-particles, the studies found that the collision probability of photons with nanocomposite materials increases, resulting in a higher attenuation coefficient and better shielding performance. These studies indicated that polymer nanocomposites can be used to produce customizable radiation shielding materials with high photon attenuation abilities [10, 23-27].

Polypropylene is a polymer made from monomer propylene. It is a thermoplastic polymer that can be used in packaging, and electrical insulation, and has excellent chemical resistance [28].

According to two studies, filling polypropylene with nanoparticle materials such as nano-SiO2 and nano-CaCO3 enhanced its mechanical performance [29, 30]. Additionally, another study found that filling polypropylene with iron nanoparticles altered its intermolecular interactions, morphology, and supramolecular structure [31]. Nanomaterials with high atomic numbers can be incorporated into polymers to fabricate radiation shielding materials that can replace lead [22], thus, adding iron nanoparticles to polypropylene may be effective for using it as a radiation shielding material. This study aims to investigate the Gamma radiation attenuation ability of polymer nanocomposite (nano-iron with polypropylene) by using the Geant4 simulation tool and EpiXS database at an energy ranging between 0.03-2 MeV. Also, the neutron radiation shielding properties of these glasses were evaluated by evaluating the effective removal cross-section ΣR/ρ (cm^2/g), effective removal cross-section ΣR(cm^{-1}), Half value layer Δ0,5 (cm) at energy 0.25 MeV, 0.5 MeV,1 MeV, 2 MeV, 3 MeV, 4.5 MeV, 5.5 MeV.

2. Materials and method

2.1. Polypropylene and Iron Nanoparticles synthesis

The isotactic polypropylene has a density of 0.9 g/ml at 250C, a refractive index of n_{20}/D 1.49, a transition temperature of -26 °C, and an average molecular weight of 250000 by GPC, and a melting point of 1890 ^{0}C. The electro-explosive technique was used to create iron nanoparticles. Isotactic polypropylene was dissolved in toluene at 1200C to produce the polymer nanocomposite composites. For an hour, iron nanoparticles were swirled into the polymer solution at varied volume contents (0.1, 0.3, 0.5, 1, 2, and 5 %). The mixture was placed in a petri dish and allowed to dry throughout the day. To thoroughly eliminate the solvent, nanocomposites have also been dried in a vacuum oven for three to four hours. By hot-pressing

these samples at the polypropylene melting temperature and a pressure of 10 MPa, the thin nanocomposite film was produced. Following hot pressing, the film was cooled with water at a rate of 2000 films per minute. Additionally, it was discovered that a 5% volume concentration of iron nanoparticles is the threshold for nanocomposites with PP and Fe filling.

Table 1. Chemical compositions of nanocomposites PP-Fe filling and their densities.

Sample code	Chemical composition of compounds (wt.%)		ρ(g.cm^{-3})
	$PP(C_3H_6)$	Fe	
PP-$Fe_{0.1}$	0.999	0.001	0.911
PP-$Fe_{0.3}$	0.997	0.003	0.925
PP-$Fe_{0.5}$	0.995	0.005	0.939
PP-Fe_1	0.99	0.01	0.974
PP-Fe_2	0.98	0.02	1.044
PP-Fe_5	0.95	0.05	1.253

2.2. Gamma attenuation

The intensity of gamma photons after passing through a mass per unit area (x) layer of a material (I) relates to the initial intensity (I_0) through the following equation where (μ_m) is the mass attenuation coefficient of the material [32]:

$$I = I_0 e^{-\mu_m x} \quad (1)$$

The linear attenuation coefficient could be found from the mass attenuation coefficient (μ) using the relation:

$$\mu = \mu_m \rho \quad (2)$$

Where (ρ) is the density of the material [33, 34]. The linear attenuation coefficient is used to determine the half value layer (HVL) of the material which is a very important property of any shielding material and could be found using the following equation [33, 34]:

$$HVL = \frac{\ln 2}{\mu} \tag{3}$$

The total atomic cross section as well as the total electronic cross-section for the element can be calculated by Equations (4 and 5) Where (N_A) is Avogradro's number, (A_i) is the atomic weight of an element of the compound, (f_i) is the number of atoms of element (i) relative to the total number of atoms of all elements in the compound, (Z_i) is the atomic number of the ith element in the compound. [35]:

$$\sigma_{t.a} = \frac{\mu_m}{N_A \sum_i^n (w_i / A_i)} \tag{4}$$

$$\sigma_{t.el} = \frac{1}{N_A} \sum_i^n \frac{f_i A_i}{Z_i} (\mu_{mt})_i \tag{5}$$

The effective atomic number (Z_{eff}) of the compound equals the ratio between the total atomic cross-section and the total electronic cross-section as shown in equation (6) while the effective electron density can be found using equation (7) [34, 36]:

$$Z_{eff} = \frac{\sigma_{t,a}}{\sigma_{t,el}} \tag{6}$$

$$N_{eff} = \frac{\mu_m}{\sigma_{t,el}} \tag{7}$$

2.3. Neutron attenuation

The neutron attenuation is described by the neutron removing cross section (Σ_R) which is the probability of the neutron reactions within the material and is given by equation (8) [37]:

$$\Sigma_R = \sum_i \rho_i \left(\Sigma_R / \rho\right)_i \quad (8)$$

Where (ρ_i) is the partial density, (Σ_R/ρ) is the mass removal cross section, which can be calculated for any compound by equation (9) Where (A) is the atomic weight and (Z) is the atomic number.

[8]:

$$\frac{\Sigma_R}{\rho} = 0.206 A^{-1/3} Z^{-0.294} \quad (9)$$

The Mean free Path (λ) which is the distance that the neutron travels without interactions is given by equation (10) [37-38]:

$$\lambda = \frac{1}{\Sigma_R} \quad (10)$$

3. Monte Carlo simulation

Geant4(G4) is a very powerful Monte Carlo based toolkit; which is utilized in nuclear physics, nuclear engineering and medical physics [39]. It was used to evaluate the gamma and neutron shielding properties of the investigated samples. A Geant4 code was developed to study the interactions of both; gammas and neutrons in the energy range between 30 and 2000 keVs. The gamma linear attenuation coefficients, half value layers, mean free paths, effective atomic densities and effective electron densities were all estimated from Geant4 at all the studied energies. Then they were validated by comparing to the results obtained from EpiXS which is a Windows-based program for photon attenuation, dosimetry and shielding, based on EPICS2017 and EPDL9 databases that allows obtaining the photon cross section data for any sample [40]. Geant4 was then used to estimate the neutron removal cross sections and mean free paths of neutrons at all studied energies within the studied samples.

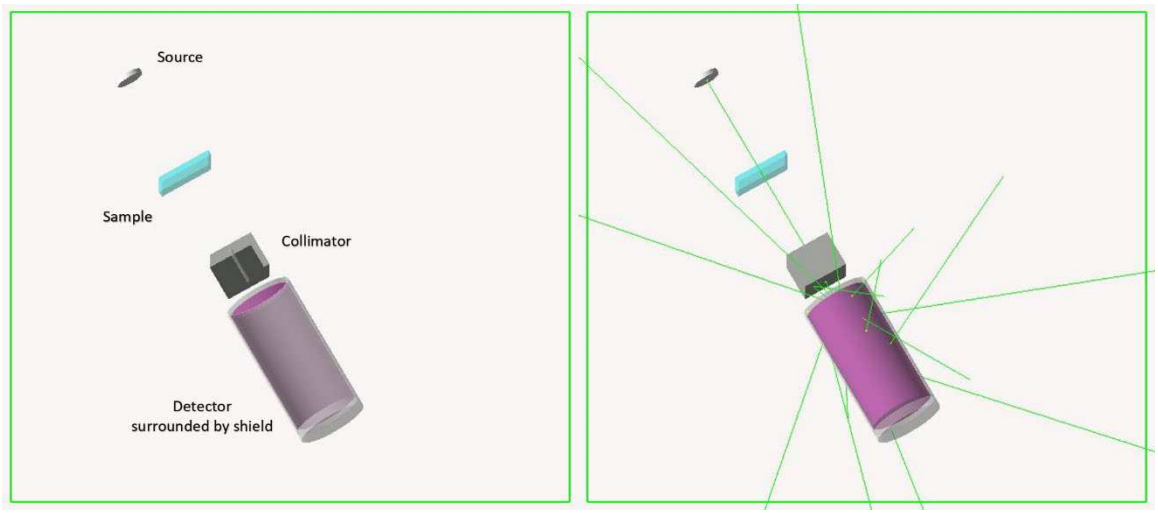

Figure 1.*Geant4* simulation code visualization

4. Results and discussion

4.1. Gamma attenuation in the investigated samples

The Geant4 code was used to evaluate the gamma radiation shielding properties of nanocomposites made of samples of isotactic polypropylene and iron nanoparticles at energies ranging from 30 to 2000 KeV, including PP-Fe $_{0.1}$, PP-Fe $_{0.3}$, PP-Fe $_{0.5}$, PP-Fe $_{1}$, PP-Fe $_{2}$, and PP-Fe $_{5}$. **Table.1** shows how increasing the amount of Fe nanoparticles can increase the density of the PP-Fe. **Fig. 1** depicts the geometry used in this experiment to perform the Geant4 simulation. **Table 2** shows the μ_m values computed by EpiXS software and simulated by Geant4. With incoming photon energies ranging from 30 to 2000 KeV, **Fig. 2** shows a variety of (μ_m) values for the PP-Fe $_{0.1}$, PP-Fe $_{0.3}$, PP-Fe $_{0.5}$, PP-Fe $_{1}$, PP-Fe $_{2}$, and PP-Fe $_{5}$. The fluctuation in the μ_m values with photon energy in the PP-Fe $_{0.1}$, PP-Fe $_{0.3}$, PP-Fe $_{0.5}$, PP-Fe $_{1}$, PP-Fe $_{2}$, and PP-Fe $_{5}$ samples can be explained by the well-known partial photon interaction mechanisms. To examine how μ_m changes with photon energy, one can use the photon and material interaction techniques.

At low (E<100 KeV), medium (100<E<1000KeV), and high (E > 1000 KeV) energies, respectively, photoelectric absorption, Compton scattering, and pair production are the three most common photon interaction modes. At energies below 100 KeV, the photoelectric effect is proportional to $Z^{4-5}/E^{3.5}$. In the intermediate energy range (100<E < 1000 KeV), the values of μ_m steadily drop with increasing photon energy, and the variance of these radiation parameters becomes independent of input photon energy. As the energy increases, photoelectric absorption becomes less likely to happen and Compton scattering replaces it as the main photon process. The variation virtually becomes energy independent when pair creation takes control, E> 1000 KeV, and μ_m values start to drastically decline as a function of photon energy. According to Fig. 2, the μ_m values for PP-Fe $_{0.1}$, PP-Fe $_{0.3}$, PP-Fe $_{0.5}$, PP-Fe $_{1}$, PP-Fe $_{2}$, and PP-Fe $_{5}$ decreases as photon energy increases. According to **fig. 2**, the mass attenuation coefficients of the PP-Fe samples increased as the density of the samples increased with increasing Fe concentration. Accordingly, among the other PP-Fe samples, sample PP-Fe$_5$ had the highest μ_m value equal to 0.835939 cm^2/g at a low energy level of 30 KeV. As seen in **Fig. 2**, the simulation and computation findings for the current polymer samples are substantially identical. With increasing photon energy, the (μ_m) values for all polymer PP-Fe $_{0.1}$, PP-Fe $_{0.3}$, PP-Fe $_{0.5}$, PP-Fe $_{1}$, PP-Fe $_{2}$, and PP-Fe $_{5}$ samples drop. For PP-Fe $_{0.1}$, PP-Fe $_{0.3}$, PP-Fe $_{0.5}$, PP-Fe $_{1}$, PP-Fe $_{2}$, and PP-Fe $_{5}$, the μ_m are 0.046048-0.253940 cm^2/g, 0.046741-0.272499 cm^2/g,0.047433- 0.291503 cm^2/g, 0.049163-0.340953 cm^2/g, 0.052612-0.448173 cm^2/g, and 0.062871-0.835939 cm^2/g.

Table 2. Gamma mass attenuation coefficients of the investigated samples as found by Geant4 and EpiXS.

Energy	**PP-Fe$_{0.1}$**			**PP-Fe$_{0.3}$**			**PP-Fe$_{0.5}$**		
(keV)	**EpiXS**	**G4**	**% diff**	**EpiXS**	**G4**	**% diff**	**EpiXS**	**G4**	**% diff**

	Mass attenuation coefficient ($cm^2.g^{-1}$)								
30	0.253940	0.251753	0.86%	0.272499	0.270377	0.78%	0.291503	0.289447	0.71%
40	0.210452	0.209908	0.26%	0.220005	0.219370	0.29%	0.229749	0.229021	0.32%
50	0.191507	0.192024	-0.27%	0.197698	0.198155	-0.23%	0.203988	0.204382	-0.19%
60	0.180351	0.181126	-0.43%	0.184995	0.185773	-0.42%	0.189697	0.190477	-0.41%
80	0.166397	0.166763	-0.22%	0.169723	0.170084	-0.21%	0.173072	0.173429	-0.21%
100	0.156761	0.156595	0.11%	0.159542	0.159374	0.11%	0.162334	0.162164	0.10%
150	0.139741	0.138911	0.59%	0.141969	0.141127	0.59%	0.144200	0.143346	0.59%
200	0.127669	0.126845	0.65%	0.129642	0.128805	0.65%	0.131615	0.130766	0.65%
300	0.110796	0.110501	0.27%	0.112477	0.112178	0.27%	0.114157	0.113853	0.27%
400	0.099180	0.099348	-0.17%	0.100677	0.100847	-0.17%	0.102172	0.102345	-0.17%
500	0.090528	0.090945	-0.46%	0.091891	0.092315	-0.46%	0.093253	0.093683	-0.46%
600	0.083728	0.084255	-0.63%	0.084987	0.085522	-0.63%	0.086245	0.086788	-0.63%
800	0.073525	0.074069	-0.74%	0.074630	0.075182	-0.74%	0.075733	0.076294	-0.74%
1000	0.066081	0.066540	-0.69%	0.067073	0.067539	-0.69%	0.068065	0.068538	-0.70%
1500	0.053747	0.053937	-0.35%	0.054554	0.054748	-0.35%	0.055361	0.055557	-0.36%
2000	0.046048	0.046061	-0.03%	0.046741	0.046755	-0.03%	0.047433	0.047448	-0.03%

Energy (keV)	PP-Fe_1			PP-Fe_2			PP-Fe_5		
	EpiXS	G4	% diff	EpiXS	G4	% diff	EpiXS	G4	% diff
	Mass attenuation coefficient ($cm^2.g^{-1}$)								
30	0.340953	0.339077	0.55%	0.448173	0.446710	0.33%	0.835718	0.835939	-0.03%
40	0.254946	0.253975	0.38%	0.308925	0.307423	0.49%	0.499157	0.495687	0.70%
50	0.220141	0.220371	-0.10%	0.254291	0.254155	0.05%	0.371192	0.369649	0.42%
60	0.201698	0.202484	-0.39%	0.226764	0.227555	-0.35%	0.310218	0.310985	-0.25%
80	0.181545	0.181889	-0.19%	0.198928	0.199241	-0.16%	0.254364	0.254536	-0.07%
100	0.169364	0.169190	0.10%	0.183636	0.183453	0.10%	0.227958	0.227752	0.09%
150	0.149786	0.148903	0.59%	0.161005	0.160063	0.59%	0.194871	0.193758	0.57%
200	0.136550	0.135669	0.65%	0.146427	0.145481	0.65%	0.175968	0.174830	0.65%
300	0.118355	0.118039	0.27%	0.126738	0.126399	0.27%	0.151669	0.151257	0.27%
400	0.105908	0.106087	-0.17%	0.113364	0.113555	-0.17%	0.135497	0.135725	-0.17%
500	0.096654	0.097100	-0.46%	0.103441	0.103919	-0.46%	0.123575	0.124147	-0.46%
600	0.089387	0.089951	-0.63%	0.095656	0.096259	-0.63%	0.114245	0.114967	-0.63%
800	0.078489	0.079071	-0.74%	0.083986	0.084610	-0.74%	0.100280	0.101030	-0.75%
1000	0.070540	0.071031	-0.70%	0.075477	0.076004	-0.70%	0.090110	0.090744	-0.70%
1500	0.057374	0.057579	-0.36%	0.061391	0.061611	-0.36%	0.073296	0.073564	-0.37%
2000	0.049163	0.049178	-0.03%	0.052612	0.052630	-0.03%	0.062845	0.062871	-0.04%

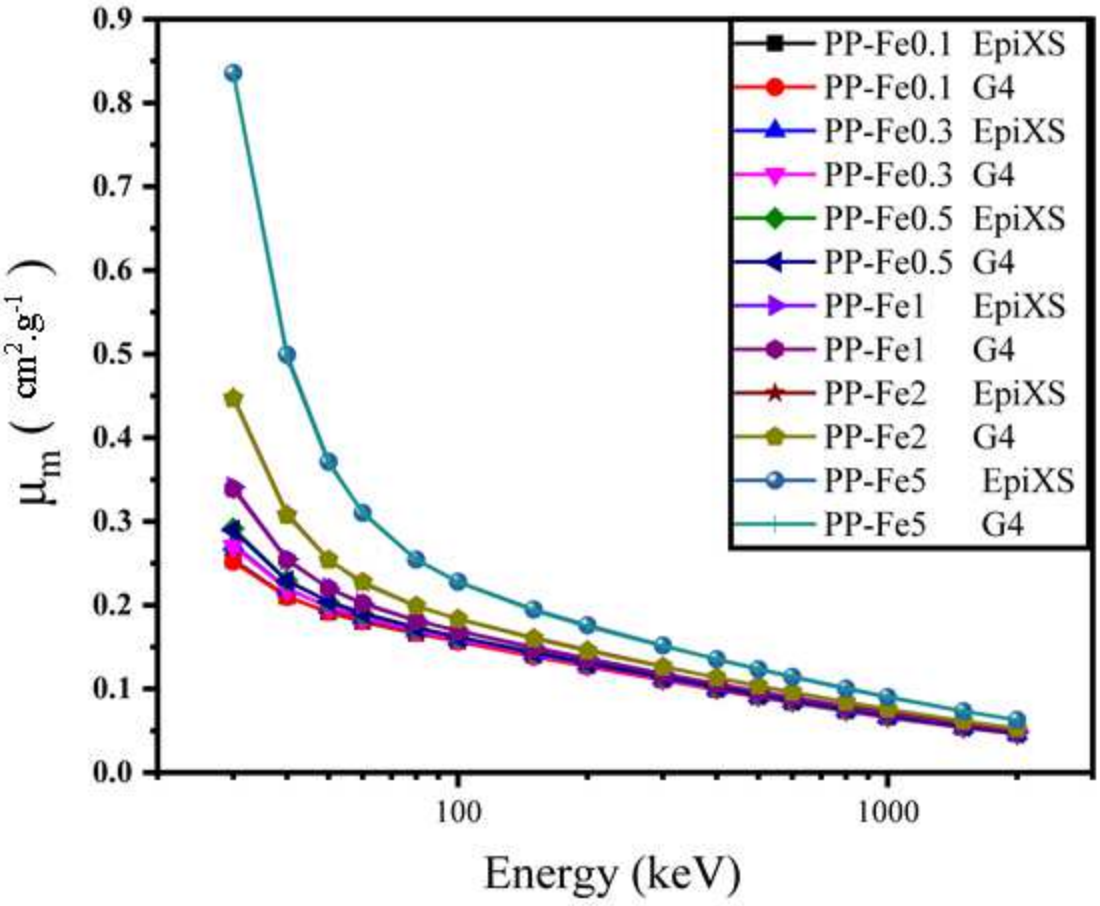

Fig 2. The variation of μ_m versus incident photon energy range between 30- 2000 KeV for the PP-Fe $_{0.1}$ to PP-Fe $_5$ samples.

The linear attenuation coefficient values were calculated. It was observed that in the low and medium energies, the linear attenuation coefficients behave similarly to the mass attenuation coefficients. The linear attenuation coefficient (μ) values were determined using the mass attenuation coefficient (μ_m) data, as shown in **Table 3**. **Figure 3** shows the μ values of the PP-Fe polymer samples with incident photon energies ranging from 30 to 2000 KeV; the linear attenuation attenuation coefficients (μ) in this figure behave similarly to the mass attenuation coefficients (μ_m). LACs for PP-Fe $_{0.1}$, PP-Fe $_{0.3}$, PP-Fe $_{0.5}$, PP-Fe $_1$, PP-Fe $_2$, and PP-Fe $_5$ samples

range from 0.0419497-0.2313393 cm^{-1}, 0.0432354-0.2520616 cm^{-1}, 0.0445396-0.2737213 cm^{-1}, 0.0478848-0.3320882 cm^{-1}, 0.0549269-0.4678926 cm^{-1},and 0.0787448-1.0471547 cm^{-1}. At energies ranging from 30 to 2000 KeV, PP-Fe_5 has the highest LAC values.

Table 3. Gamma linear attenuation coefficients of the investigated samples as found by EpiXS.

Energy (keV)	**PP-$Fe_{0.1}$**	**PP-$Fe_{0.3}$**	**PP-$Fe_{0.5}$**	**PP-Fe_1**	**PP-Fe_2**	**PP-Fe_5**
30	0.2313393	0.2520616	0.2737213	0.3320882	0.4678926	1.0471547
40	0.1917218	0.2035046	0.2157343	0.2483174	0.3225177	0.6254437
50	0.1744629	0.1828707	0.1915447	0.2144173	0.2654798	0.4651036
60	0.1642998	0.1711204	0.1781255	0.1964539	0.2367416	0.3887032
80	0.1515877	0.1569938	0.1625146	0.1768248	0.2076808	0.3187181
100	0.1428093	0.1475764	0.1524316	0.1649605	0.191716	0.2856314
150	0.1273041	0.1313213	0.1354038	0.1458916	0.1680892	0.2441734
200	0.1163065	0.1199189	0.1235865	0.1329997	0.1528698	0.2204879
300	0.1009352	0.1040412	0.1071934	0.1152778	0.1323145	0.1900413
400	0.090353	0.0931262	0.0959395	0.1031544	0.118352	0.1697777
500	0.082471	0.0849992	0.0875646	0.094141	0.1079924	0.1548395
600	0.0762762	0.078613	0.0809841	0.0870629	0.0998649	0.143149
800	0.0669813	0.0690328	0.0711133	0.0764483	0.0876814	0.1256508
1000	0.0601998	0.0620425	0.063913	0.068706	0.078798	0.1129078
1500	0.0489635	0.0504625	0.051984	0.0558823	0.0640922	0.0918399
2000	0.0419497	0.0432354	0.0445396	0.0478848	0.0549269	0.0787448

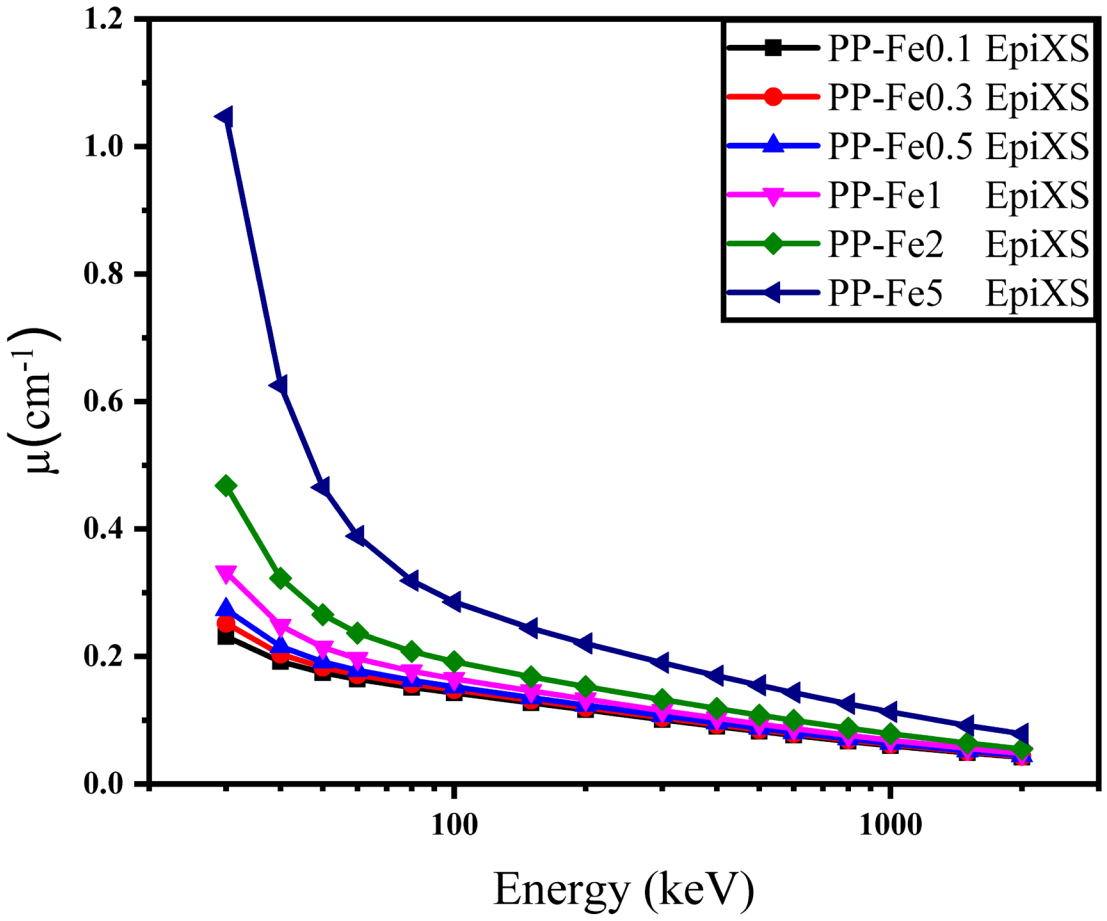

Fig 3. Linear attenuation coefficient values versus incident photon energy range between 30-2000 KeV for the PP-Fe $_{0.1}$ to PP-Fe $_{5}$ samples.

HVL is a crucial consideration when evaluating a material's gamma shielding potential. **Tables 4** displayed the HVL values for PP-Fe$_{0.1}$ to PP-Fe$_{5}$. **Figure 4** plot the HVL values vs photon energy. **Figure 4** show how the half-value layer grows as the incident photon energy rises. As a result, the half-value layer is impacted by photon energy. **Figure 4** show that HVL values are low in energy area 30 KeV, then rapidly increase as photon energy increases, reaching their highest values at energy region 2000 KeV. According to **Figure 4**, the highest values of the HVL

were obtained at 2000 KeV and ranged from 16.51977 cm to 2.99 cm. According to the data, the polymer sample PP-Fe_5 with the highest Fe content had the lowest HVL values.

Table 4. Gamma half value layers of the investigated PP-$Fe_{0.1}$ to PP-Fe_5 samples as found by EpiXS.

	HVL(cm)					
Energy (keV)	**PP-$Fe_{0.1}$**	**PP-$Fe_{0.3}$**	**PP-$Fe_{0.5}$**	**PP-Fe_1**	**PP-Fe_2**	**PP-Fe_5**
30	2.99559945	2.74932821	2.53177212	2.08679488	1.48110909	0.66179336
40	3.61461295	3.40532801	3.21228458	2.79078304	2.14871928	1.10801336
50	3.97219175	3.78956383	3.61795385	3.23201481	2.61036806	1.48999069
60	4.21790023	4.04978075	3.89051577	3.527546	2.92724199	1.7828515
80	4.57161202	4.41418776	4.26423205	3.91913285	3.33685104	2.17433531
100	4.85262613	4.69587437	4.54630065	4.20100478	3.61472208	2.42620406
150	5.44366023	5.27713226	5.11802475	4.7501033	4.12281049	2.83814742
200	5.95839652	5.77890799	5.60740926	5.21053807	4.53326984	3.14302956
300	6.86579411	6.66082123	6.46494888	6.01156667	5.23752232	3.6465766
400	7.66991858	7.44151285	7.22330158	6.71808526	5.85541357	4.08180717
500	8.40295295	8.15302031	7.91416007	7.36129879	6.417118	4.47560288
600	9.08540183	8.81533869	8.55724006	7.95975895	6.9393776	4.84111012
800	10.3461751	10.0387135	9.74501432	9.06495144	7.90361612	5.51528346
1000	11.5116679	11.1697582	10.8428586	10.0864612	8.7946408	6.1377497
1500	14.1533951	13.7329836	13.3310303	12.4010697	10.8125475	7.54574091
2000	16.5197734	16.0285229	15.5591923	14.4722448	12.6167624	8.80058279

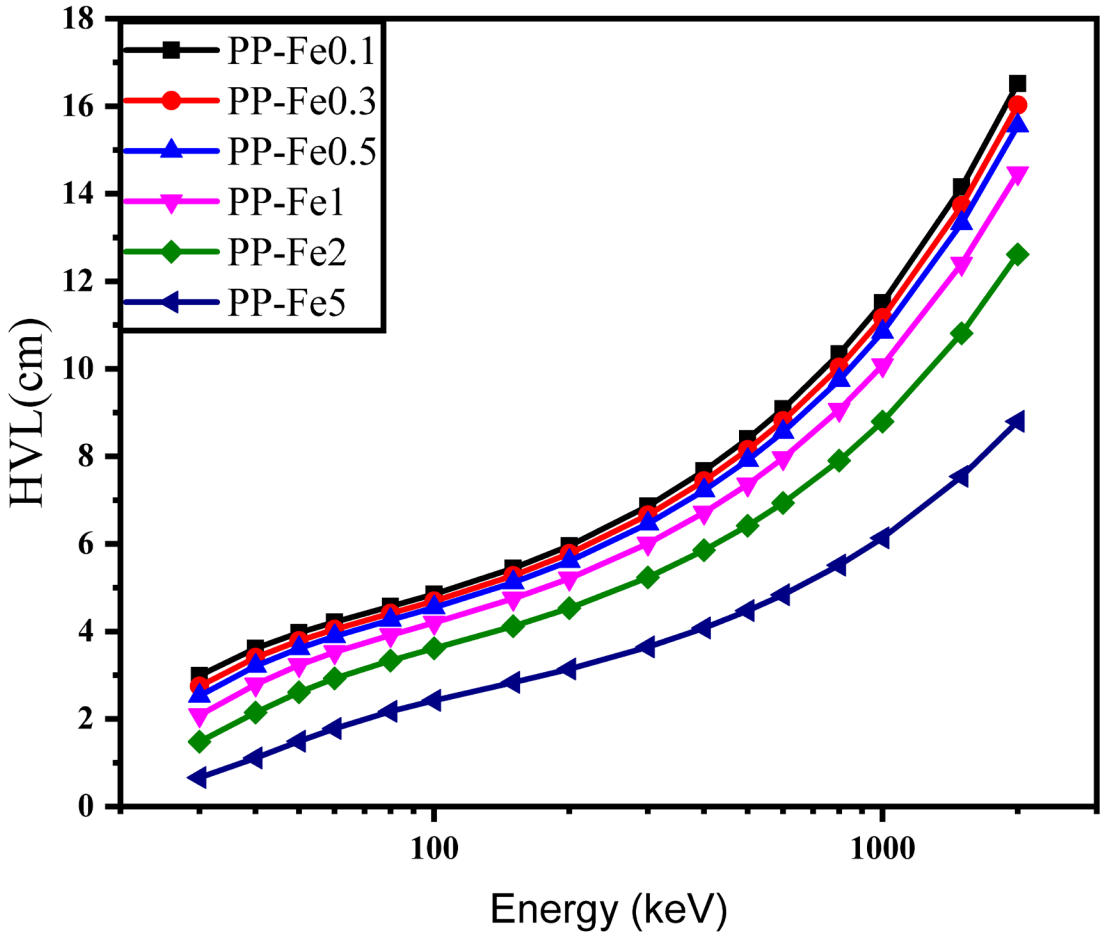

Fig 4. HVL values for the studied PP-$Fe_{0.1}$ to PP-Fe_5 polymer samples at different photon energies 30-2000 KeV.

The Z_{eff} values of the PP-$Fe_{0.1}$ to PP-Fe_5 samples between 30 and 2000 KeV are shown in **Fig. 5**. The glass under consideration is better for radiation protection objectives the higher the Z_{eff}. The figure illustrates how the photoelectric phenomena causes all of the PP-$Fe_{0.1}$ to PP-Fe_5 samples to have relatively high Z_{eff} at low energy. The Z_{eff} decreases as energy increases, suggesting that photons have a better likelihood of interacting with PPFe polymer samples at low energies[44]. According to **Figure 5**, at all energies, the Z_{eff} increased as the number of FeO nanoparticles

increased. If we look at the PPFe$_{0.1}$ and PPFe$_5$, it becomes evident that the Fe effectively increases the Z_{eff}. For these two samples, the Zeff at 30 KeV is 3.164 and 6.721 , whereas, at 2000 KeV these values are 2.676 and 2.78. We can infer from the data in the Z_{eff} figure that the photons interact with the PP-Fe$_{0.1}$ and PP-Fe$_5$ samples, respectively, with the lowest and best penetrating abilities.

Table 5. Effective atomic numbers(Z_{eff}) of the investigated PP-Fe$_{0.1}$ to PP-Fe$_5$ samples as found by Geant4 and EpiXS.

Energy (keV)	PP-Fe$_{0.1}$	PP-Fe$_{0.3}$	PP-Fe$_{0.5}$	PP-Fe$_1$	PP-Fe$_2$	PP-Fe$_5$
30	3.164	3.327	3.488	3.883	4.645	6.721
40	2.91	2.991	3.073	3.274	3.674	4.836
50	2.806	2.853	2.9	3.017	3.251	3.953
60	2.757	2.787	2.817	2.893	3.045	3.508
80	2.713	2.729	2.745	2.785	2.866	3.116
100	2.696	2.706	2.717	2.743	2.797	2.963
150	2.68	2.686	2.692	2.708	2.74	2.838
200	2.675	2.68	2.685	2.698	2.724	2.804
300	2.672	2.676	2.681	2.692	2.714	2.783
400	2.671	2.675	2.679	2.69	2.711	2.777
500	2.67	2.674	2.678	2.689	2.71	2.774
600	2.67	2.674	2.678	2.688	2.709	2.773
800	2.67	2.674	2.678	2.688	2.708	2.772
1000	2.669	2.673	2.677	2.687	2.708	2.771
1500	2.671	2.675	2.679	2.689	2.709	2.772
2000	2.676	2.68	2.684	2.694	2.715	2.78

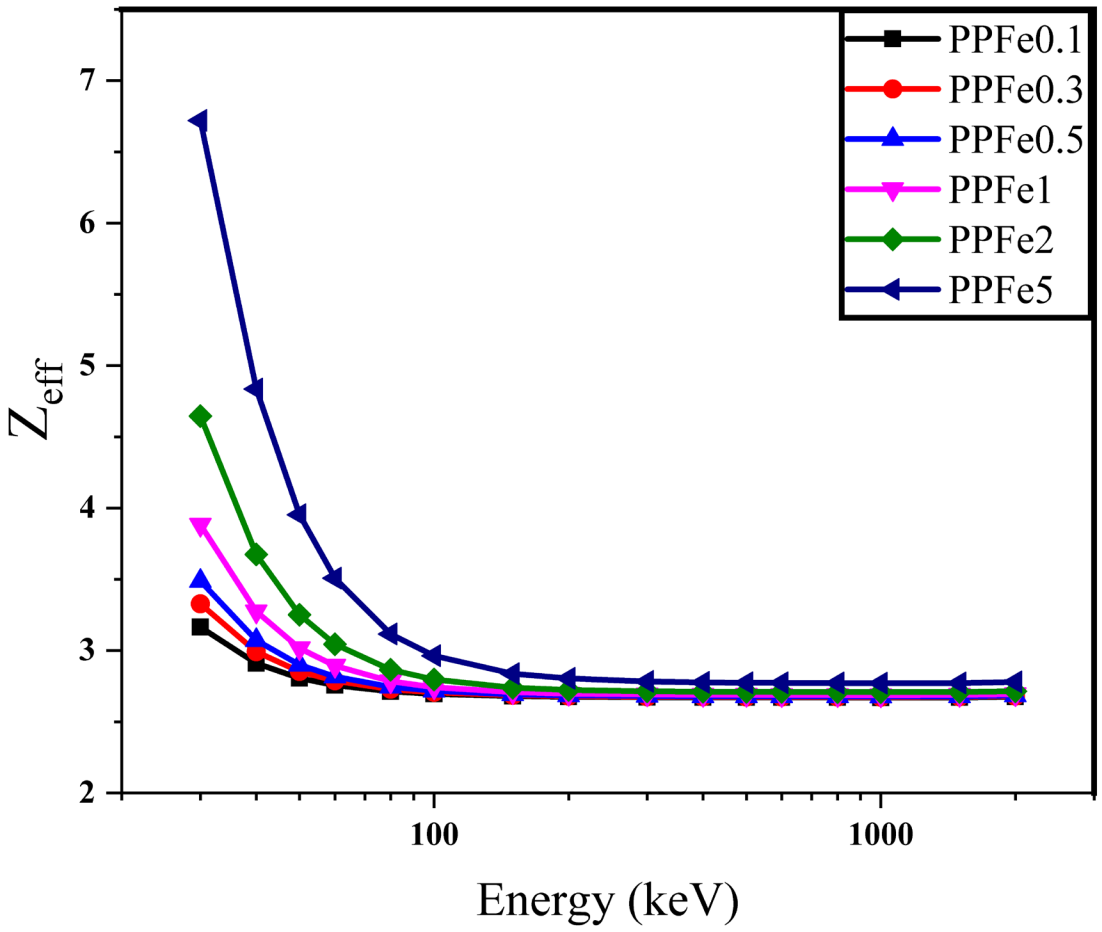

Fig. 5. The effective atomic number values for the PP-$Fe_{0.1}$ to PP-Fe_5 samples.

Fig. 6 displays the fluctuation in effective electron densities (Ne) of PP-$Fe_{0.1}$ to PP-Fe_5 samples at various gamma-ray energy. The N_{eff} values in the PP-$Fe_{0.1}$ to PP-Fe_5 samples are higher at low energy and exponentially drop at high energy. This shows that PP-$Fe_{0.1}$ to PP-Fe_5 samples interact with gamma rays of lower energies more frequently than those of higher energies, which results in more electrons being produced because the results are produced at lower energies. Z_{eff} and N_{eff} findings show similar tendencies, with both values decreasing exponentially as energy increases.

Table 6. Effective electron densities (N_{eff}) of the investigated samples as found by Geant4 and EpiXS.

Energy (keV)	PP-$Fe_{0.1}$	PP-$Fe_{0.3}$	PP-$Fe_{0.5}$	PP-Fe_{1}	PP-Fe_{2}	PP-Fe_{5}
30	4.071	4.273	4.472	4.956	5.873	8.26
40	3.745	3.842	3.939	4.179	4.645	5.944
50	3.611	3.665	3.718	3.85	4.111	4.859
60	3.547	3.58	3.612	3.692	3.85	4.312
80	3.491	3.505	3.519	3.554	3.624	3.83
100	3.469	3.476	3.483	3.501	3.536	3.641
150	3.449	3.45	3.452	3.456	3.464	3.488
200	3.443	3.443	3.443	3.443	3.444	3.446
300	3.438	3.438	3.437	3.435	3.431	3.42
400	3.437	3.436	3.435	3.433	3.428	3.413
500	3.436	3.435	3.434	3.431	3.426	3.41
600	3.436	3.435	3.434	3.431	3.425	3.408
800	3.435	3.434	3.433	3.43	3.424	3.406
1000	3.435	3.434	3.433	3.43	3.424	3.406
1500	3.437	3.436	3.434	3.431	3.425	3.407
2000	3.444	3.442	3.441	3.439	3.433	3.416

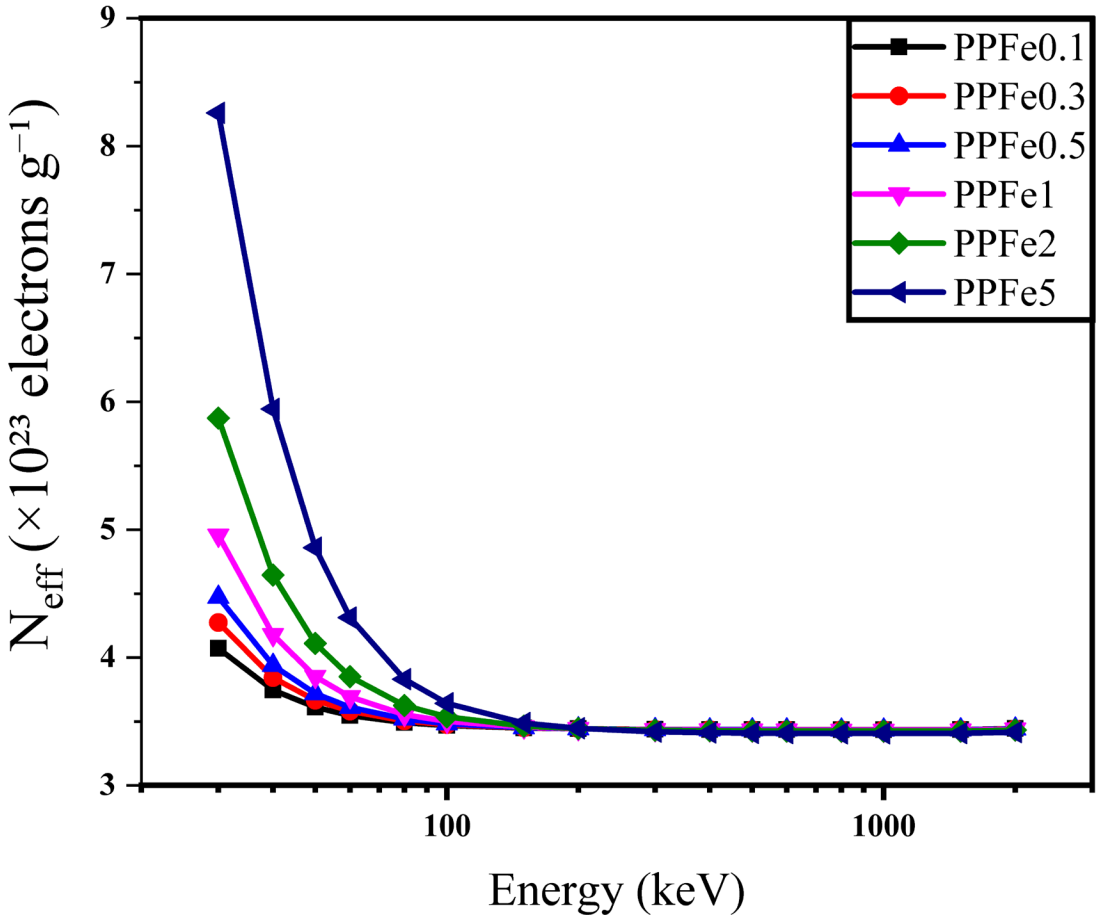

Fig. 6. The effective electron densities values for the PP-$Fe_{0.1}$-PP-Fe_5 samples.

4.2. Neutron attenuation in the investigated samples

Figure 7 shows the ∑R(cm^{-1}) for the PP-$Fe_{0.1}$ to PP-Fe_5 system. It is stated plainly that ∑R(cm^{-1}) values increased from 0.84947 to 1.10650 cm^{-1}, while the Fe content increased from 0.1 to 5 mol%.The PP-Fe_5 polymer sample which containing 5 mol% of Fe, has the highest ∑R value (1.10650 cm^{-1}). It means the PP-Fe_5 polymer sample is the most effective ones among the other samples for fast neutron shielding. Based on the ∑R estimation, fast neutron mean free path (mfp, cm) of the examined glass samples was computed. All of the chosen PP-$Fe_{0.1}$ to PP-Fe_5 samples' mfp variations were compared to one another, and the results are shown in Fig. 8. It can be seen that sample coded as PP-$Fe_{0.1}$ had the highest mfp value, while sample coded as PP-Fe_5 had the lowest value, meaning that the fast neutrons in PP-Fe0.1 polymer sample travelled farther between two collisions than they did in the other types of PP-Fe samples.

Table 7. Effective removal cross sections and mean free paths of neutrons in the investigated samples as found by Geant4.

Energy	PP-$Fe_{0.1}$			PP-$Fe_{0.3}$			PP-$Fe_{0.5}$		
(keV)	Σ_R (cm^2/g)	Σ_R (cm^{-1})	MFP (cm)	Σ_R (cm^2/g)	Σ_R (cm^{-1})	MFP (cm)	Σ_R (cm^2/g)	Σ_R (cm^{-1})	MFP (cm)
0.25	0.92819	0.84947	1.1772	0.92641	0.85776	1.1658	0.92461	0.86815	1.1519
0.5	0.68159	0.61805	1.6180	0.68026	0.62752	1.5936	0.67893	0.63676	1.5704
1	0.48148	0.43912	2.2773	0.48057	0.44429	2.2508	0.47966	0.4522	2.2114
2	0.32184	0.29330	3.4094	0.32125	0.29663	3.3712	0.32065	0.30149	3.3169
3	0.24720	0.22626	4.4196	0.24677	0.22811	4.3839	0.24634	0.23126	4.3241
4.5	0.22248	0.20188	4.9535	0.22212	0.20563	4.8630	0.22176	0.20794	4.8091
5.5	0.18109	0.16477	6.0691	0.18081	0.16694	5.9900	0.18052	0.16906	5.9151

Energy	PP-Fe_1			PP-Fe_2			PP-Fe_5		
(keV)	Σ_R (cm^2/g)	Σ_R (cm^{-1})	MFP (cm)	Σ_R (cm^2/g)	Σ_R (cm^{-1})	MFP (cm)	Σ_R (cm^2/g)	Σ_R (cm^{-1})	MFP (cm)
0.25	0.92013	0.90056	1.1104	0.91116	0.94998	1.0527	0.88428	1.10650	0.90375
0.5	0.67562	0.65793	1.5199	0.66898	0.69882	1.4310	0.64907	0.81458	1.22763
1	0.47738	0.46501	2.1505	0.47281	0.49349	2.0264	0.45915	0.57562	1.73726
2	0.31918	0.31209	3.2042	0.31622	0.33307	3.0024	0.30733	0.38603	2.59047
3	0.24525	0.24017	4.1637	0.24309	0.25411	3.9354	0.23665	0.29663	3.3712
4.5	0.22085	0.21497	4.6518	0.21904	0.22887	4.3693	0.21358	0.26715	3.74322
5.5	0.17981	0.17512	5.7105	0.17839	0.18700	5.3477	0.17411	0.21791	4.58905

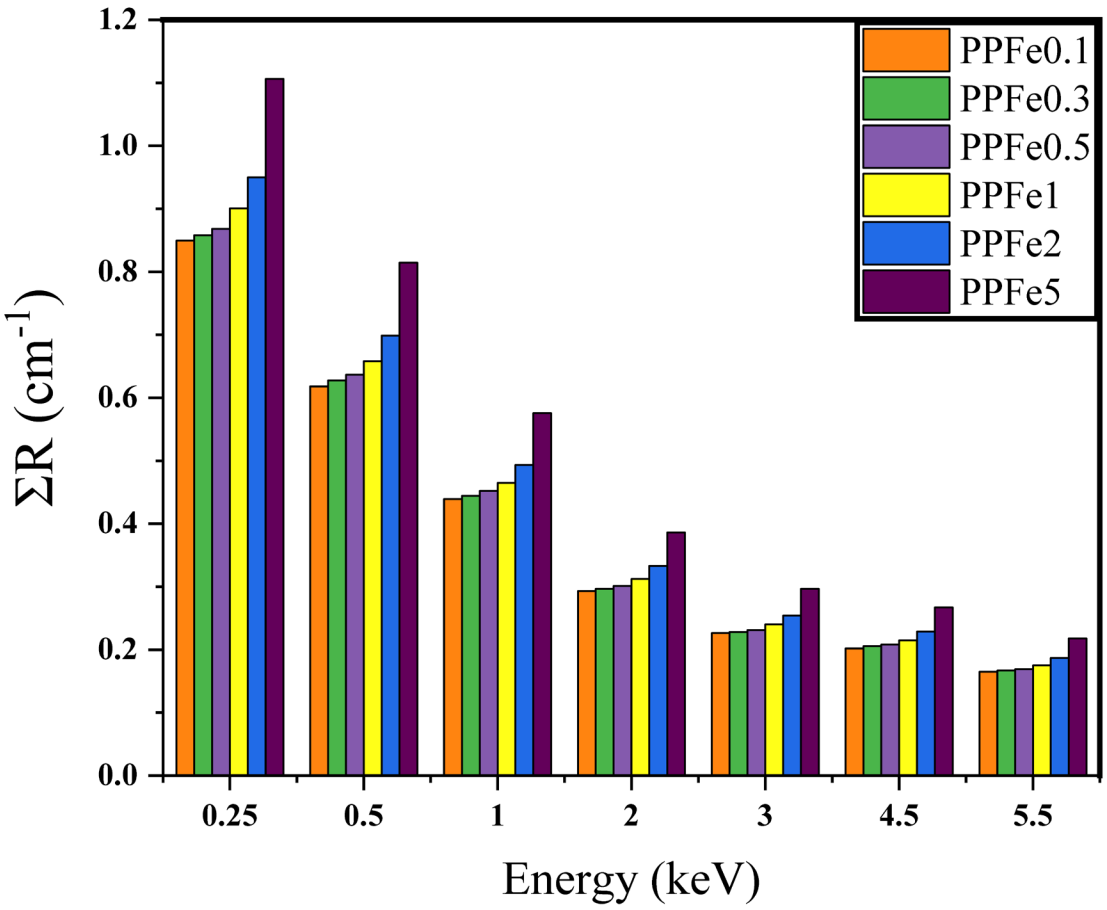

Fig.7. Fast neutron removal cross sections ΣR(cm^{-1}) for the PP-$Fe_{0.1}$-PP-Fe_5 samples.

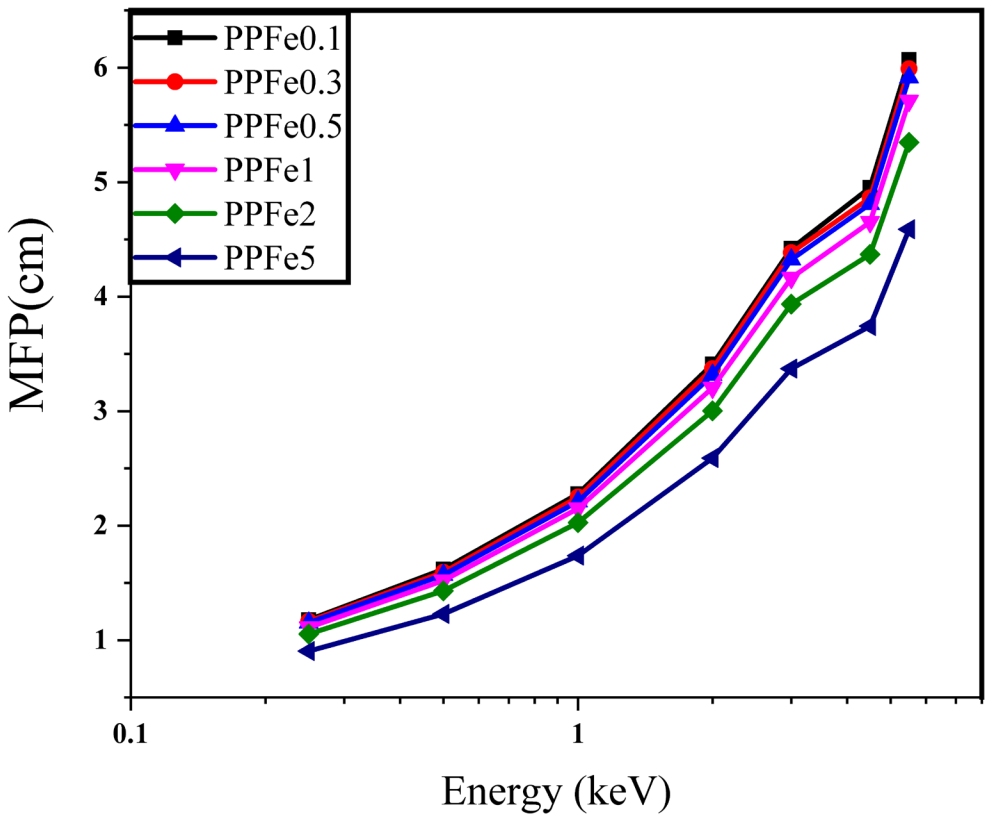

Fig. 8. Fast neutron mean free path versus for the PP-$Fe_{0.1}$-PP-Fe_5 samples.

5. Conclusion

By using the Geant4 Monte Carlo code, we examined the gamma-neutron shielding capabilities of polymer nanocomposite materials based on polypropylene with varied iron nanoparticles contents (0.1, 0.3, 0.5, 1, 2, and 5 %). A comparison was made between the founded results and those predicted by EpiXS. A remarkable agreement was found between the values obtained from Geant4 and EpiXS software. Results showed that the gamma-ray shielding effectiveness of PP-Fe polymer samples increased with an increase in the Fe nanoparticle content. The best gamma-ray shielding ability is found in the PP-Fe_5 sample. PP-Fe_5 also has the lowest fast neutron mean

free path value and the highest ∑R value (1.10650 cm^{-1}). PP-Fe_5 has therefore a better shielding efficiency against gamma-neutrons.

Conflicts of interests

All authors certify that they have no affiliations with or involvement in any organization or entity with any financial interest or non-financial interest in the subject matter or materials discussed in this manuscript.

References

1. Mikhailova, A., Tashlykov, O., 2020. The ways of implementation of the optimization principle in the personnel radiological protection. Phys. Atom. Nucl. 83, 1718–1726.
2. Tashlykov, O., Shcheklein, S., Russkikh, I., Seleznev, E., Kozlov, A., 2017. Composition optimization of homogeneous radiation-protective materials for planned irradiation conditions. Atom. Energy 121, 303–307.
3. Russkikh, I., Seleznev, E., Tashlykov, O., Shcheklein, S., 2015. Experimental and theoretical study of organometallic radiation-protective materials adapted to radiation sources with a complex isotopic composition. Phys. Atom. Nucl. 78, 1451–1456.
4. Tashlykov, O.L., Shcheklein, S.E., Luk'yanenko, V.Y., Mikhajlova, A.F., Russkikh, I.M., Seleznyov, E.N., Kozlov, A.V., 2015. The optimization of radiation protection composition. Izvestiya Wysshikh Uchebnykh Zawedeniy. Yadernaya Energetika 4, 36–42. https://doi.org/10.26583/npe.2015.4.04 , 2015 .
5. More, C.V., R.R. Bhosale, and P.P. Pawar, *Detection of new polymer materials as gamma-ray-shielding materials.* Radiation Effects and Defects in Solids, 2017. **172**(5-6): p. 469-484.
6. Dixon, R.L., *On the primary barrier in diagnostic x-ray shielding.* Medical physics, 1994. **21**(11): p. 1785-1793.
7. Sayyed, M., G. Lakshminarayana, and M. Mahdi, *Evaluation of radiation shielding parameters for optical materials.* Chalcogenide Lett, 2017. **14**(2): p. 43-47.
8. Singh, V., et al., *Determination of mass attenuation coefficient for some polymers using Monte Carlo simulation.* Vacuum, 2015. **119**: p. 284-288.
9. Thuyavan, Y.L., et al., *Preparation and characterization of TiO2-sulfonated polymer embedded polyetherimide membranes for effective desalination application.* Desalination, 2015. **365**: p. 355-364.
10. Nambiar, S. and J.T. Yeow, *Polymer-composite materials for radiation protection.* ACS applied materials & interfaces, 2012. **4**(11): p. 5717-5726.

11. Wang, Y., et al., *Enhanced photon shielding efficiency of a flexible and lightweight rare earth/polymer composite: A Monte Carlo simulation study.* Nuclear Engineering and Technology, 2020. **52**(7): p. 1565-1570.
12. Aghamiri, M., et al., *A novel design for production of efficient flexible lead-free shields against X-ray photons in diagnostic energy range.* Journal of Biomedical Physics and Engineering, 2011. **1**(1).
13. Takano, Y., et al., *Experimental and theoretical studies on radiation protective effect of a lighter non-lead protective apron.* Nihon Hoshasen Gijutsu Gakkai Zasshi, 2005. **61**(7): p. 1027-1032.
14. Yue, K., et al., *A new lead-free radiation shielding material for radiotherapy.* Radiation protection dosimetry, 2009. **133**(4): p. 256-260.
15. Almurayshid, M., et al., *Development of new lead-free composite materials as potential radiation shields.* Materials, 2021. **14**(17): p. 4957.
16. Sallam, O., et al., *Impact of radiation on CoO-doped borate glass: lead-free radiation shielding.* Applied Physics A, 2022. **128**(1): p. 1-16.
17. Alavian, H., A. Samie, and H. Tavakoli-Anbaran, *Experimental and Monte Carlo investigations of gamma ray transmission and buildup factors for inorganic nanoparticle/epoxy composites.* Radiation Physics and Chemistry, 2020. **174**: p. 108960.
18. Atashi, P., et al., *Efficient, flexible and lead-free composite based on room temperature vulcanizing silicone rubber/W/Bi2O3 for gamma ray shielding application.* Journal of Materials Science: Materials in Electronics, 2018. **29**(14): p. 12306-12322.
19. Shameem, M.M., et al., *A brief review on polymer nanocomposites and its applications.* Materials Today: Proceedings, 2021. **45**: p. 2536-2539.
20. Abdalsalam, A.H., et al., *A study of gamma attenuation property of UHMWPE/Bi2O3 nanocomposites.* Chemical Physics, 2019. **523**: p. 92-98.
21. Shik, N.A. and L. Gholamzadeh, *X-ray shielding performance of the EPVC composites with micro-or nanoparticles of WO3, PbO or Bi2O3.* Applied radiation and isotopes, 2018. **139**: p. 61-65.
22. Mansouri, E., et al., *Shielding characteristics of nanocomposites for protection against X- and gamma rays in medical applications: effect of particle size, photon energy and nano-particle concentration.* Radiation and Environmental Biophysics, 2020. **59**(4): p. 583-600.
23. Wozniak, A., et al., *Modern approaches to polymer materials protecting from ionizing radiation.* Journal Port Science Research, 2018.
24. Hashim, A. and A. Hadi, *Novel lead oxide polymer nanocomposites for nuclear radiation shielding applications.* Ukrainian Journal of Physics, 2017. **62**(11): p. 978-978.
25. Maksoud, M.A., et al., *Gamma radiation shielding properties of poly (vinyl butyral)/Bi2O3@ BaZrO3 nanocomposites.* Materials Chemistry and Physics, 2021. **268**: p. 124728.
26. Kawady, N.A., et al., *Fabrication, characterization, and gamma ray shielding properties of PVA-based polymer nanocomposite.* Journal of Materials Science, 2022: p. 1-16.
27. Kim, S., et al., *Tungsten nanoparticle anchoring on boron nitride nanosheet-based polymer nanocomposites for complex radiation shielding.* Composites Science and Technology, 2022. **221**: p. 109353.
28. Maddah, H.A., *Polypropylene as a promising plastic: A review.* Am. J. Polym. Sci, 2016. **6**(1): p. 1-11.

29. Rong, M.Z., et al., *Structure–property relationships of irradiation grafted nano-inorganic particle filled polypropylene composites.* Polymer, 2001. **42**(1): p. 167-183.
30. Rong, M.Z., et al., *Irradiation graft polymerization on nano-inorganic particles: An effective means to design polymer-based nanocomposites.* Journal of Materials Science Letters, 2000. **19**(13): p. 1159-1161.
31. Ramazanov, M., et al., *The magnetic polymer nanocomposite materials based on polypropylene and iron nanoparticles: Synthesis and structure.* J. Ovanic. Res, 2016. **12**: p. 193-32. Hubbell J (1982) Photon mass attenuation and energy-absorption coefficients. The International Journal of Applied Radiation and Isotopes 33:1269-1290. doi: 10.1016/0020-708x(82)90248-4.
32. Aladailah, M. W., Tashlykov, O. L., Shirmanov, I. A., Strugov, E. D., Marashdeh, M. W., Abdelmunem, E. M., & Eke, C. (2022). Photon absorption capabilities of SiO2–Na2O–P2O5–CaO–MgO glasses. Radiation Physics and Chemistry, 190, 109814.
33. Aladailah, M. W., Tashlykov, O. L., Shirmanov, I. A., Strugov, E. D., Sayyed, M. I., Marashdeh, M. W., ... & Al-Maaitah, A. F. (2022). Radiation attenuation properties of novel glass system using experimental and Geant4 simulation. Radiation Physics and Chemistry, 199, 110404.
34. Aladailah, M. W., Shirmanov, I. A., Strugov, E. D., Tashlykov, O. L., Eke, C., & Yildirim, A. (2022, June). Assessment of radiation-protective properties of Y2O3-MnO2-Al2O3-SiO2-CaO using Phy-X software and Geant4 simulation code. In AIP Conference Proceedings (Vol. 2466, No. 1, p. 060026). AIP Publishing LLC.
35. Aladailah, M. W., Tashlykov, O. L., Marashdeh, M. W., & Akhdar, H. (2022). Photon, neutron absorption capabilities of Y2O3-Al2O3-P2O5 glasses. Radiation Effects and Defects in Solids, 1-16.
36. Kaewkhao J, Laopaiboon J, Chewpraditkul W (2008) Determination of effective atomic numbers and effective electron densities for Cu/Zn alloy. Journal of Quantitative Spectroscopy and Radiative Transfer 109:1260-1265. doi: 10.1016/j.jqsrt.2007.10.007.
37. Olukotun S, Mann K, Gbenu S, Ibitoye F, Oladejo O, Joshi A, Tekin H, Sayyed M, Fasasi M, Balogun F, Korkut T (2019) Neutron-shielding behaviour investigations of some clay-materials. Nuclear Engineering and Technology 51:1444-1450. doi: 10.1016/j.net.2019.03.019.
38. El Abd A, Mesbah G, Mohammed N, Ellithi A (2017) A simple Method for Determining the Effective Removal Cross Section for Fast Neutrons. Journal of Radiation and Nuclear Applications 2:53-58. doi: 10.18576/jrna/020203.
39. Agostinelli, S.; Allison, J.; Amako, K.; Apostolakis, J.; Araujo, H.; Arce, P.; Asai, M.; Axen, D.; Banerjee, S.; Barrand, G.; Behner, F.; Bellagamba, L.; Boudreau, J.; Broglia, L.; Brunengo, A.; Burkhardt, H.; Chauvie, S.; Chuma, J.; Chytracek, R.; Cooperman, G.; Cosmo, G.; Degtyarenko, P.; Dell'Acqua, A.; Depaola, G.; Dietrich, D.; Enami, R.; Feliciello, A.; Ferguson, C.; Fesefeldt, H.; Folger, G.; Foppiano, F.; Forti, A.; Garelli, S.; Giani, S.; Giannitrapani, R.; Gibin, D.; Gómez Cadenas, J.; González, I.; Gracia Abril, G.; Greeniaus, G.; Greiner, W.; Grichine, V.; Grossheim, A.; Guatelli, S.; Gumplinger, P.; Hamatsu, R.; Hashimoto, K.; Hasui, H.; Heikkinen, A.; Howard, A.; Ivanchenko, V.; Johnson, A.; Jones, F.; Kallenbach, J.; Kanaya, N.; Kawabata, M.; Kawabata, Y.; Kawaguti, M.; Kelner, S.; Kent, P.; Kimura, A.; Kodama, T.; Kokoulin, R.; Kossov, M.; Kurashi-ge, H.; Lamanna, E.; Lampén, T.; Lara, V.; Lefebure, V.; Lei, F.; Liendl, M.; Lockman, W.; Longo, F.; Magni, S.; Maire, M.; Medernach, E.; Minamimoto, K.; Mora

de Freitas, P.; Morita, Y.; Murakami, K.; Nagamatu, M.; Nartallo, R.; Nieminen, P.; Nishimura, T.; Ohtsubo, K.; Okamura, M.; O'Neale, S.; Oohata, Y.; Paech, K.; Perl, J.; Pfeiffer, A.; Pia, M.; Ranjard, F.; Rybin, A.; Sadilov, S.; Di Salvo, E.; Santin, G.; Sasaki, T.; Savvas, N.; Sawada, Y.; Scherer, S.; Sei, S.; Sirotenko, V.; Smith, D.; Starkov, N.; Stoecker, H.; Sulkimo, J.; Takahata, M.; Tanaka, S.; Tcherniaev, E.; Safai Tehrani, E.; Tropeano, M.; Truscott, P.; Uno, H.; Urban, L.; Urban, P.; Verderi, M.; Walkden, A.; Wander, W.; Weber, H.; Wellisch, J.; Wenaus, T.; Williams, D.; Wright, D.; Yamada, T.; Yoshida, H.; Zschiesche, D. (2003) Geant4—a simulation toolkit. Nuclear Instruments and Methods in Physics Research Section A: Accelerators, Spectrometers, Detectors and Associated Equipment 506, 250-303.

40. Hila F, Asuncion-Astronomo A, Dingle C, Jecong J, Javier-Hila A, Gili M, Balderas C, Lopez G, Guillermo N, Amorsolo A (2021) EpiXS: A Windows-based program for photon attenuation, dosimetry and shielding based on EPICS2017 (ENDF/B-VIII) and EPDL97 (ENDF/B-VI.8). Radiation Physics and Chemistry 182:109331. doi: 10.1016/j.radphyschem.2020.109331.
41. Gaikwad D., Sayyed M., Obaid S.S., Issa S.A., Pawar P., (2018), Gamma ray shielding properties of TeO2-ZnF2-As2O3-Sm2O3 glasses. Journal of Alloys and Compounds 765, 451-458.
42. El-Mallawany R., Sayyed M., Dong M., Rammah Y., (2018), Simulation of radiation shielding properties of glasses contain PbO. Radiation Physics and Chemistry 151, 239-252.
43. Kavaz E., Tekin H., Agar O., Altunsoy E., Kilicoglu O., Kamislioglu M., Abuzaid M., Sayyed M., (2019b), The Mass stopping power/projected range and nuclear shielding behaviors of barium bismuth borate glasses and influence of cerium oxide. Ceramics International 45, 15348-15357.
44. Gaikwad, D. K., Sayyed, M. I., Botewad, S. N., Obaid, S. S., Khattari, Z. Y., Gawai, U. P., ... & Pawar, P. P. (2019). Physical, structural, optical investigation and shielding featuresof tungsten bismuth tellurite based glasses. Journal of Non-Crystalline Solids, 503, 158-168.